Journal of Materials Chemistry A

ROYAL SOCIETY OF CHEMISTRY

PAPER

View Article Online
View Journal | View Issue

Cite this: J. Mater. Chem. A, 2023, 11, 9922

Optimization of thermal exfoliation of graphitic carbon nitride for methylparaben photocatalytic degradation under simulated solar radiation

Jorge Plaza,[a] Amaya Arencibia[b] and María José López-Muñoz *[a]

Previous studies have shown that the exfoliation of graphitic carbon nitride (g-C_3N_4) is essential to obtain materials with good photocatalytic properties. However, in most studies the influence of exfoliation variables was investigated in an unsystematic way by changing the levels of one factor at a time. In this work, a full factorial design 3^2 was employed to evaluate the influence of temperature and time used in the thermal exfoliation of bulk g-C_3N_4 obtained from urea (bulk-U), on the photocatalytic performance for 5 mg L^{-1} methylparaben degradation under simulated solar radiation. Based on the thermal stability of the starting bulk-U, the levels of the design were set in the range of 400 to 450 °C for temperature and 2 to 6 h for time. The results showed an enhancement in the photocatalytic activity with an increase in both factors, obtaining the maximum response at $T = 450$ °C and $t = 6$ h. An economic evaluation at the laboratory scale including the main costs derived from the synthesis stage and the photocatalytic degradation procedure was also performed, comparing all the exfoliated materials. The total expenses could be minimized without compromising good photocatalytic activity with the material obtained by exfoliation of bulk-U at 450 °C for 2 h. Detailed characterization of the materials was carried out by XRD, FT-IR, adsorption–desorption of N_2, TEM, SEM, UV-Vis DR, and PL spectroscopy. It was inferred that the enhancement of the photocatalytic performance induced by the exfoliation was mainly related to the consequent increase in the surface area and the improvement in the separation of photogenerated charge pairs derived from the unpacking of the stacked layers.

Received 22nd February 2023
Accepted 12th April 2023

DOI: 10.1039/d3ta01109g

rsc.li/materials-a

1. Introduction

In recent years polymeric graphitic carbon nitride (g-C_3N_4) has attracted much attention as a metal-free semiconductor for photocatalytic applications since it shows a band gap *ca.* 2.7 eV which makes it active under visible-spectrum light, is non-toxic and exhibits a relatively high stability to photo-corrosion and acid or base solutions. Moreover, g-C_3N_4 can be easily synthesized by the polycondensation of a variety of organic precursors containing both carbon and nitrogen such as urea, cyanamide, dicyandiamide or melamine.[1,2] However, bulk g-C_3N_4 also has a number of shortcomings that limit its photocatalytic efficiency, among which are: (i) a high rate of electron–hole pair recombination, (ii) a low surface area and (iii) a moderate water oxidation ability due to the energy position of the upper limit of the valence band (VB) at about 1.4 V *vs.* NHE.[3] The latter means that the photo-generated holes of g-C_3N_4 are able to attain only oxygen evolution from water oxidation, instead of the formation of oxidant hydroxyl radicals ($HO^{\bullet}$) hence limiting its applications in photocatalytic depuration processes.[4]

To overcome the above-mentioned disadvantages and enhance the photocatalytic performance of g-C_3N_4 different strategies have been proposed, such as the exfoliation of the 2D-stacked layers that build the graphite-like structure of bulk g-C_3N_4. Exfoliation into single-layered nanosheets, feasible due to the weak van der Waals forces between the layers, leads to both an increase in the specific surface area, hence providing a higher number of exposed catalytic centres, and an improvement in the electron transport ability along the in-plane direction.[5] As a result, the exfoliated materials show higher photocatalytic activity compared to their bulk counterparts.

Different approaches have been previously reported to attain the exfoliation of bulk g-C_3N_4 including mechanical, supercritical, hydrothermal, liquid-phase and thermal exfoliation methods.[4,6] Among them, thermal exfoliation has attracted great attention as it is a simple and effective procedure. Previous studies have reported that the experimental variables of the etching process, such as time or temperature, can have a significant influence on the optical and electronic properties of the materials obtained.[7] However, to the best of our knowledge, the experiments that showed such an effect were

[a]Departamento de Tecnología Química y Ambiental, ESCET, Universidad Rey Juan Carlos, 28933, Móstoles, Madrid, Spain. E-mail: mariajose.lopez@urjc.es
[b]Departamento de Tecnología Química, Energética y Mecánica, ESCET, Universidad Rey Juan Carlos, 28933, Móstoles, Madrid, Spain

performed in an unsystematic way by changing the levels of one factor at a time.

On this basis, in the present work a systematic approach using factorial experimental design was carried out to screen the influence of the temperature and time of thermal exfoliation of bulk g-C_3N_4 on the photocatalytic properties of the obtained materials. Methylparaben (MeP, $C_8H_8O_3$) was evaluated as the target molecule in the simulated solar light-mediated photocatalytic reactions. MeP is the methyl ester of *p*-hydroxybenzoic acid, widely present as a preservative in formulations of cosmetics and personal care products due to its broad antimicrobial and anti-fungal properties. Despite being substantially removed in wastewater treatment plants (WWTPs), the presence of MeP in aquatic systems including freshwater, brackish and marine water, sediments, and biota has been reported.[8] This is a matter of concern since previous studies have warned of the potential estrogenicity and endocrine-disrupting properties of parabens,[9] which is what makes it important to investigate their removal from the aqueous medium.

2. Experimental

2.1. Synthesis of g-C_3N_4 materials

The bulk g-C_3N_4 sample (bulk-U) was synthesized by thermal polymerization using urea as a precursor. Briefly, 15 g urea were dissolved in 20 mL of Milli-Q® water and the homogeneous solution was placed in three covered crucibles, which were heated in a muffle furnace in two consecutive steps at 400 °C for 2 h and 450 °C for 2 h at a 5 °C min^{-1} heating rate. After cooling to room temperature, the solid obtained was ground and sieved to a particle size <200 μm. The exfoliation of bulk-U was carried out by thermal etching at different temperatures in the range of 400 to 450 °C for 2, 4, or 6 h in an air atmosphere. The solids obtained were labelled as U*xxx*-*y*, where "*xxx*" represents the temperature applied and "*y*" the duration of treatment. As an example, the sample U425-4 was obtained by exfoliation of bulk-U at 425 °C for 4 h.

2.2. Characterization

X-ray diffraction (XRD) patterns were acquired using Philips X-PERT MPD equipment with Cu Kα radiation ($\lambda = 1.5414$ Å) as an X-ray source. Data were recorded in the range of 10 to 80° at a 0.01° step size. The adsorption–desorption isotherms were obtained on a Micromeritics Tristar 3000, using N_2 at −196 °C. Prior to the analysis, the samples were subjected to two degasification steps under nitrogen at 90 °C and 200 °C for 5 h. BET surface area (S_{BET}) was determined using adsorption data at a relative pressure (P/P_0) between 0.05 and 0.2. The morphology and structure of the synthesised materials were determined by scanning electron microscopy (SEM) with a JEOL JSM-7900F at 1–30 kV and transmission electron microscopy (TEM), performed on a STEM JEOL F200 microscope operating at 200 kV. The total content of C, H, N and O was evaluated using a CHNS-O analyzer FLASH 2000 Thermo Scientific. The optical properties of the samples were investigated by UV-Vis diffuse reflectance (DR) spectroscopy using a Varian Cary 500 Scan UV-Vis-NIR spectrophotometer equipped with an integrating sphere. The wavelength range analysed was 200 to 800 nm with a spectral scan rate of 100 nm min^{-1}. The energy band gap values were obtained by extrapolating a linear fitting in the Tauc plot. Photoluminescence (PL) spectra were obtained with an Agilent Cary Eclipse spectrophotometer using an excitation wavelength of 350 nm. Time-resolved fluorescence emission spectra were recorded at room temperature with a Mini-tau system from Edinburgh Instruments, using an EPL-375 picosecond pulsed diode laser. As an excitation source, an EPL-375 picosecond pulsed diode laser with emission at 372 nm was used and the emission was recorded with a band pass filter at 420 nm. Infrared spectra of the samples were recorded with 4 cm^{-1} resolution and 64 scans in the wavenumber range of 4000–500 cm^{-1} using a PerkinElmer Frontier IR spectrophotometer equipped with an ATR module. Thermograms of the bulk material were analysed using a thermogravimetric analyser model TGA/DSC 1 with a 5 °C min^{-1} heating ramp and a constant air gas flow of 100 mL min^{-1}.

2.3. Photocatalytic reactions

The photocatalytic reactions for MeP degradation were conducted in a reactor of 1 L capacity placed in a solar-radiation simulator (Solarbox 1500). The solar chamber was provided with a 1500 W Xenon lamp and a λ <300 nm cut-off filter, obtaining an average light intensity of 329 W m^{-2} in the 300–800 nm range (StellarNet Spectrometer). The initial concentration of MeP was set at 5 mg L^{-1} with a loading of the g-C_3N_4 catalyst of 0.25 g L^{-1}. The suspension was magnetically stirred and continuously saturated with an air flow. Aliquots taken over reaction time were filtered through a 0.22 μm syringe-driven PTFE filter for analysis in HPLC equipment (Agilent 1260 Infinity II) provided with a reversed phase column (Agilent Poroshell 120 EC-C18). Methanol–H_2O (30 : 70, v/v) was used as the mobile phase with a flow rate of 0.8 mL min^{-1}.

2.4. Factorial experimental design

Multivariate experimental design was carried out following the methodology of response surface. Analysis of the experimental data was carried out using the statistical graphics software system STATGRAPHICS Centurion Version XVI.

3. Results and discussion

3.1. Experimental design

Preliminary experiments were carried out using bulk-U under simulated solar radiation. This photocatalyst could effectively degrade MeP (5 mg L^{-1}) up to >99% within 220 min of irradiation. A first-order kinetic model was used to fit the experimental profile of the MeP concentration as a function of irradiation time, obtaining a kinetic constant, $k = 0.0087$ min^{-1} ($R^2 = 0.985$).

The factorial design methodology was then used to evaluate the influence of two factors on the thermal exfoliation of bulk-U, namely temperature (X_1) and duration time (X_2), on the resulting photocatalytic properties. To establish the levels of both

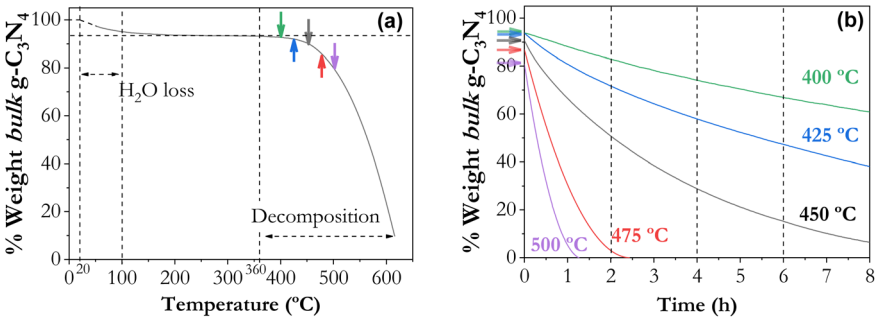

Fig. 1 Thermogravimetric analysis of bulk-U in air as a function of (a) temperature and (b) time. The arrows included in (a) indicate the starting point of the analysis in (b).

factors in the experimental design, a thermogravimetric analysis (TGA) of bulk-U was initially performed to assess its thermal stability in air (Fig. 1). Fig. 1a displays the TGA curve obtained as a function of temperature. An initial decrease in weight of *ca.* 5% within the temperature range of 20 to 100 °C is observed, which is associated with the removal of physisorbed water from the catalyst surface. Next, bulk-U exhibited a high thermal stability up to 360 °C, above which it diminished slightly up to *ca.* 450 °C. Beyond this temperature, the weight percentage decreased drastically until the decomposition of the material at over 600 °C.[10] Also, the influence of the thermal treatment duration on the mass yield of the exfoliated materials was evaluated by TG analysis in the range of 400 to 500 °C (Fig. 1b). As shown, a drastic loss of mass (>95%) was observed within 1 and 2 h at 500 and 475 °C, respectively. By contrast, a more gradual decline of the percentage weight over time, indicative of a higher thermal stability, could be noted at lower temperatures. Even though a mass loss of around 85% was observed at 450 °C after 6 h, this led to establishing the latter experimental conditions as the upper values for the temperature (X_1) and time (X_2) factors, respectively, to avoid a very scarce mass yield.

According to the above considerations a full factorial design 3^2, two factors at three levels, was proposed setting the upper and lower limits for temperature and time factors at 400 and 450 °C and 2 and 6 h, respectively. The design consisted of 11 experiments, comprising 4 factorial points, 4 axial points and 3 replications of the central point, the latter of which was used to determine the experimental error. Table 1 displays the actual values and code levels of temperature and time factors used in each experiment and the label assigned to the exfoliated samples. For each run, the experimental percentages of MeP photocatalytic elimination with simulated solar radiation after 30, 45 and 60 min were taken as design response variables (Table 1). The photocatalytic results were well fitted to a first-order kinetic model with all materials (calculated kinetic constants shown in Table 1). It is worth noting that compared with the results obtained with bulk-U indicated above (>99% MeP degradation within 220 min of irradiation) the exfoliation of the material brought out a very significant enhancement of the photocatalytic performance, attaining ≥99% MeP degradation within 60 min of irradiation in some cases.

The experimental reaction results obtained were fitted to a second-order polynomial equation (response function):

$$Y = b_0 + b_1X_1 + b_2X_2 + b_{12}X_1X_2 + b_{11}X_1^2 + b_{22}X_2^2 \quad (1)$$

where Y represents the % MeP elimination at a fixed time; X_1 and X_2 are the factors evaluated (temperature and time); b_0 is the independent coefficient; b_1 and b_2 are the linear coefficients for temperature and time; b_{12} represents the binary

Table 1 Design matrix and experimental results of the photocatalytic response (% MeP degradation at reaction times of 30, 45 and 60 min) and the calculated cost response (relative costs involved at the lab scale)

	Code		Factors			Experimental result (% MeP deg.)			Kinetic constant	
Exp.	X_1	X_2	T (°C)	t (h)	Exfoliated sample (ID)	t = 30 min	t = 45 min	t = 60 min	k (min^{-1})	Calculated relative cost (%)
1	0	0	425	4	U425-4	55.7	70.4	85.3	0.033	52.4
2	0	0	425	4	U425-4	57.8	70.4	85.6	0.036	53.5
3	0	0	425	4	U425-4	60.9	74.3	84.4	0.035	51.7
4	−1	−1	400	2	U400-2	30.3	40.2	48.0	0.011	88.8
5	−1	0	400	4	U400-4	38.7	51.3	63.0	0.025	58.2
6	−1	+1	400	6	U400-6	65.3	80.7	91.1	0.039	52.5
7	0	−1	425	2	U425-2	48.4	62.4	74.2	0.027	50.2
8	0	+1	425	6	U425-6	87.5	95.7	98.8	0.065	51.7
9	+1	−1	450	2	U450-2	68.5	82.4	93.8	0.044	40.3
10	+1	0	450	4	U450-4	92.0	98.3	99.6	0.091	57.9
11	+1	+1	450	6	U450-6	84.6	94.6	98.6	0.068	100

Table 2 Statistical models obtained for the responses analysed

Calculated response function	R^2
Photocatalytic responses	
$Y_{30} = 60.86 + 18.47X_1 + 15.03X_2 + 0.41{X_1}^2 - 4.75X_1X_2 + 2.97{X_2}^2$	$R^2 = 0.977$
$Y_{45} = 73.30 + 17.21X_1 + 14.33X_2 - 0.95\ {X_1}^2 - 7.07X_1X_2 + 3.33{X_2}^2$	$R^2 = 0.946$
$Y_{60} = 85.04 + 14.99X_1 + 12.06X_2 - 3.67\ {X_1}^2 - 9.57X_1\ X_2 + 1.48{X_2}^2$	$R^2 = 0.987$
Cost response	
$Y'_{cost} = 49.61 - 0.22X_1 + 4.15X_2 + 12.85{X_1}^2 + 24.00X_1X_2 + 5.75{X_2}^2$	$R^2 = 0.950$

interactions; and b_{11} and b_{22}, the quadratic interactions. Validation of the mathematical model was performed by the *F*-test for analysis of variance (ANOVA). For the significance of the effects and interactions of the factors on the response, a confidence level of 95% was used. The statistical significance was considered for a *P*-value <0.05 (5%).

Table 2 shows the statistical equations obtained on the dimensionless scale (−1 0 1) for the photocatalytic responses Y_{30}, Y_{45} and Y_{60}. As can be seen, the correlation coefficient values (R^2) indicate good model adequacy, corroborated by the appreciable degree of correlation between the predictive values of the model and the experimental values observed for the responses analysed (Fig. 2a).

The determination of significant factors generated among the linear, binary, and quadratic interactions was obtained from the standardized Pareto diagram (Fig. 2b). The Pareto chart shows that the first-order effects of temperature (X_1) and time (X_2) are relevant. Hence it could be inferred that an increase in these variables might enhance the efficiency of the exfoliated material for the photocatalytic degradation of MeP.

For a clearer analysis, Fig. 3 displays the response surfaces and the contour representations of the calculated polynomial functions for MeP removal at 30, 45 and 60 min of irradiation included in Table 2. As can be observed, there is an increasing trend in the response variable with the increase of both temperature and time of exfoliation of bulk-U, obtaining the maximum response at $T = 450$ °C and $t = 6$ h (U450-6).

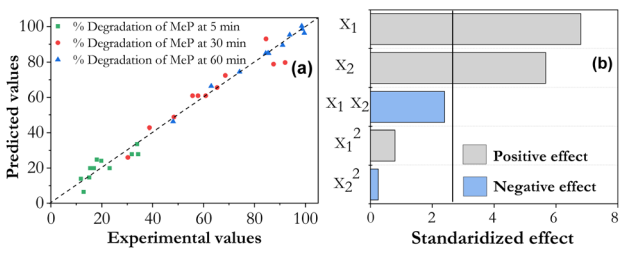

Fig. 2 (a) Correlation between predicted and experimental values for the photocatalytic degradation of MeP at different irradiation times. (b) Pareto diagram of standardized effects of the factorial design proposed for the response at 45 min of the photocatalytic reaction (Y_{45}).

Accordingly, the factorial design points to a further increase in the upper levels of both factors to improve the photocatalytic performance of the exfoliated materials. However, the thermogravimetric experiments (Fig. 1) demonstrated that such an increase in temperature or time would lead to a significant decrease in the mass yield of the catalyst thus highly increasing the costs associated with the elimination of the target pollutant.

3.2. Economic evaluation

The actual viability of a synthesized material for its use in photocatalytic applications should be linked not only to its photoactivity, but also to economic aspects ranging from the synthesis of the catalyst to the decontamination process for its use. To contemplate the latter consideration, a first approximation of global costs at the lab scale was carried out including all the materials evaluated in the factorial design shown above.

For the economic study both factors (the exfoliation temperature and time of bulk-U) were kept as in the previous section, setting the costs to attain a 99.5% degradation of MeP as the variable response (Table 1). The costs calculated were fitted to the second-order polynomial (eqn (1)) to obtain the response function, which was labelled as Y'_{cost} (Table 2). The economic assessment was composed, on the one hand, of the costs associated with the whole synthesis process including the expenses of the precursor reagent and the electrical costs for both the thermal polycondensation of urea and the post-thermal treatment of bulk-U to obtain the exfoliated material. The latter costs are mainly governed by the temperature and duration of the treatments which, in turn, determine the amount of electricity needed during the synthesis stage. On the other hand, the analysis of total expenses also considered those associated with the photocatalytic reaction as a function of its duration to attain the desired concentration of the target pollutant. The reaction time depends on the activity exhibited by the photocatalyst and includes the expenses for aeration and the electrical costs due to the irradiation within the solar simulation box and the magnetic stirring of the suspension.

Due to the variability of the costs evaluated, mainly those related to the electricity use, they have been expressed in relative terms taking as a reference the total expenses of the material that involved the highest costs, U450-6, for which a value of 100% was assigned (Table 1). Therefore, a timeless reading of the results obtained in the present work can be made. As it can be observed in Table 2 the fitting of the results to equation Y'_{cost} yielded a good regression coefficient for the estimation.

Fig. 4 displays the response surface and the contour graph expressed as relative costs. As can be seen (Fig. 4a and b), the minimum costs were estimated for an exfoliation time over 2–2.4 h and a temperature in the range of 435–450 °C, experimental conditions leading to a *ca.* 60% reduction in costs compared to the reference material, U450-6. These results and, in general, the shape of the response surface clearly show the balance between the costs associated with the synthesis stage and those derived from the photocatalytic process. To minimize the expenses of the photocatalytic stage it is necessary to get materials with higher activity.

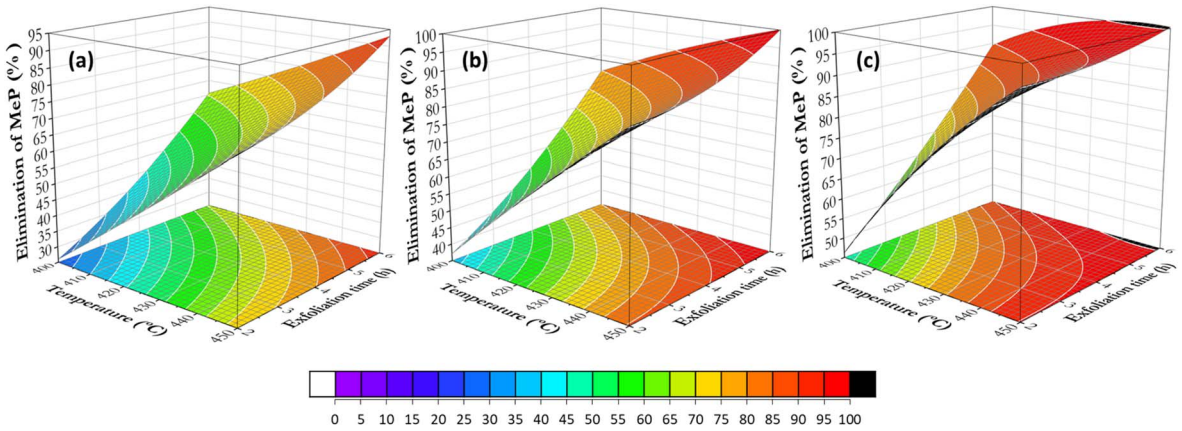

Fig. 3 Representative response and contour surfaces of the effect of temperature and exfoliation time of bulk g-C_3N_4 on the photocatalytic performance for % MeP removal (scale from 0 to 100%) at different solar irradiation times: (a) 30, (b) 45, and (c) 60 min.

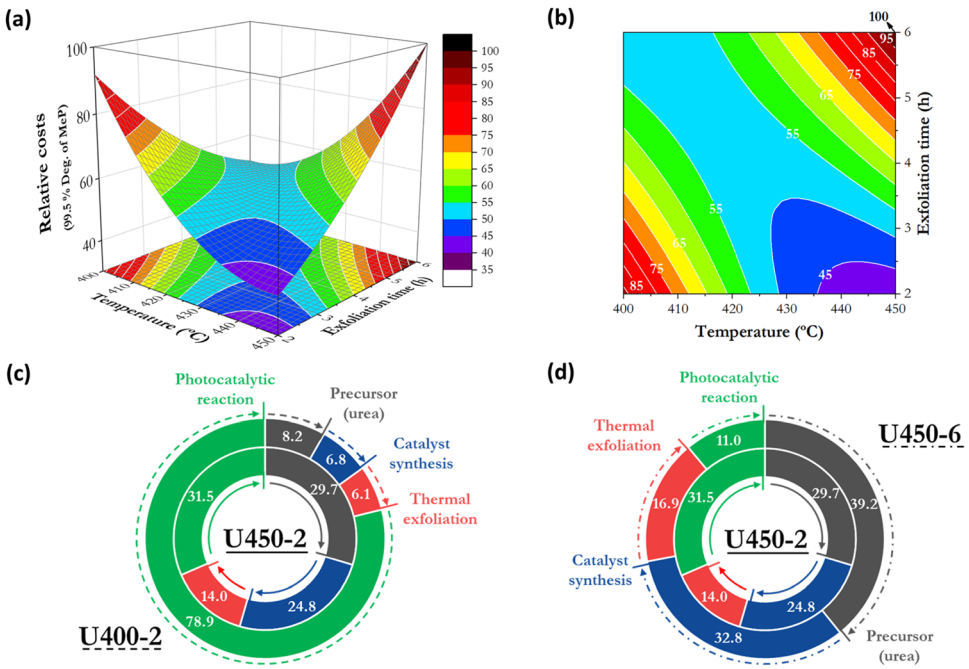

Fig. 4 (a and b) Representative response and contour surfaces of the relative costs associated with the degradation of 99.5% of MeP as a function of the effects of temperature and exfoliation time. (c and d) Breakdown of the percentages of costs associated with the material with the lowest relative cost (U450-2; the inner circle) and higher costs (U400-2 and U450-6; outer circles for c and d, respectively).

As seen in Fig. 3, the latter is associated with the increase of the exfoliation temperature and time, which leads to an increase in electricity costs in the synthesis stage. As a result, the overall cost grows up to its maximum value (U450-6). Likewise, but in the opposite direction, this occurs for the photocatalysts synthesized at the lower temperatures and times. In this case the costs of the synthesis stage are greatly decreased, but since the materials obtained show a lower photoactivity a longer irradiation time is required for attaining the degradation of MeP, hence increasing the overall costs to a value close to the reference value (92% for U400-2).

For a better understanding Fig. 4c and d show a graphical comparison between the distribution of costs calculated for the most economical material, U450-2, and the two high-cost materials, U400-2 and U450-6. For U400-2, the photocatalytic reaction accounts for 78.9% of the total cost whereas only 21.1% stands for the synthesis step. Quite the opposite, in the U450-6 material only 11.0% of costs are derived from the MeP degradation process while 89.0% are ascribed to the synthesis of the catalyst. In between them both, the optimal cost value found for U450-2 derives from a distribution of costs of 68.5% and 31.5% for the catalyst synthesis and the photocatalytic reaction, respectively.

It should be noted that the above estimation of costs is a first approach to the expenses related to laboratory scale experimentation and hence, for practical applications it would be necessary to evaluate additional aspects such as the scale-up of the synthesis of the material, the use of direct solar radiation or the reuse of the photocatalyst. Nevertheless, the economical estimation carried out shows that not only the efficiency within a certain time but also the expenses for synthesis and reactions should be considered in the development of photocatalysts.

3.3. Characterization of the photocatalysts

To understand the influence of the exfoliation variables analysed in the factorial design on the photocatalytic performance of the materials, they were characterized by XRD, N_2 adsorption–desorption isotherms, FTIR, elemental analysis, TEM, SEM, UV-Vis DR, and PL spectroscopy.

Fig. 5a displays the XRD patterns of selected samples. The weak diffraction signal at $2\theta = 13.2°$ assigned to the (1 0 0) plane is associated with the ordering of heptazine units linked by hydrogen bonds within the 2D layer of the materials. The diffraction signal at $2\theta = 27.4°$ is ascribed to the (0 0 2) plane of graphitic carbon nitrides and related to the van der Waals forces that generate the periodic stacking between layers along the *c* axis.[11–13] In comparison to the bulk-U sample the exfoliated samples showed a decrease in the intensity of both peaks, more significant for the diffraction at 27.4°. The enlarged view of the (0 0 2) peak (Fig. 5b) demonstrates that the gradual decrease of the signal, which denotes an increasing exfoliation degree, is linked to the increase of the temperature and duration of the thermal treatment (lower intensity in U450-4 and U450-6). The reduction of the intensity of the (1 0 0) signal is indicative of the breaking of intralayer H-bonds and the interlayer stacking hence proving the exfoliation achieved.[12,14,15] In turn, this is in accordance with the better photocatalytic activity shown by the latter samples in comparison to the materials exfoliated at lower temperatures, as observed in Fig. 3.

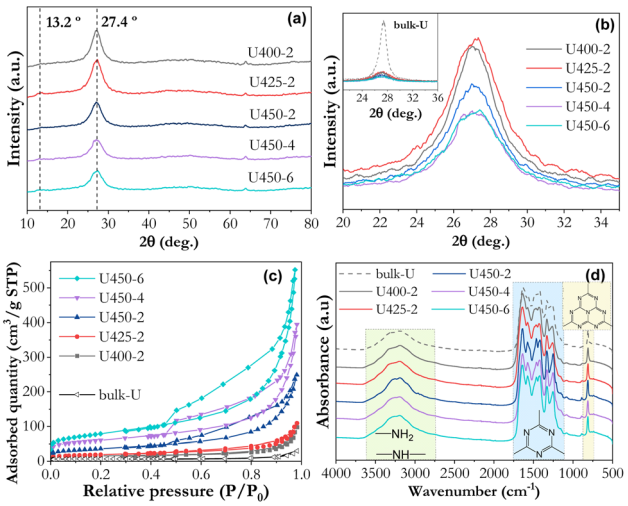

Fig. 5 (a) XRD patterns and (b) enlarged view of the (0 0 2) peak, (c) N_2 adsorption–desorption isotherms and (d) FTIR spectra of bulk-U and exfoliated materials.

The N_2 adsorption–desorption isotherms of the exfoliated materials (Fig. 5c) showed a gradual change in shape with increasing temperature and time of exfoliation. According to the classification collected by the IUPAC, the isotherms of bulk-U and samples exfoliated at 400 and 425 °C can be classified as type III isotherms. For the materials obtained at a higher temperature and time, a change to type IV isotherms was observed with an increase in adsorption at moderately high pressures along with the presence of an H3-type hysteresis loop, which indicates the development of a certain mesoporosity.[16,17]

Table 3 summarizes the BET surface area and total pore volume of representative samples. As can be observed both parameters increase with temperature and time of exfoliation. The BET surface area increases with the temperature of exfoliation from 23 $cm^2\ g^{-1}$ (bulk-U) to 49 $cm^2\ g^{-1}$ (U400-2) and 124 $cm^2\ g^{-1}$ (U450-2), being further enhanced to 279 $cm^2\ g^{-1}$ (U450-6) by increasing the exfoliation time from 2 to 6 h at 450 °C. Following a similar trend, the total pore volume increases from 0.027 (bulk-U) to 0.679 $cm^3\ g^{-1}$ (U450-6). These results confirm the success of the thermal treatment for unpacking the layers of the graphitic structure into 2D nanosheets, in agreement with the previous results,[17,18] and the significant influence of the exfoliation variables (temperature and time) on the textural properties of the resulting materials. Also, the increase in the surface area provides a higher number of active sites that can account for the improvement in the photocatalytic activity shown by the materials (Table 1).

The characteristic functional groups of the catalyst structure were probed by FTIR spectroscopy. As shown in Fig. 5d, the FTIR spectra of the bulk and exfoliated materials are quite similar despite the respective thermal treatments. In all samples a broad band centred at ~3200 cm^{-1} is observed, which is indicative of the presence of hydrogen bonding. Also in

Table 3 Summary of the textural and optical properties of bulk-U and exfoliated samples

Samples	S_{BET} ($m^2\ g^{-1}$)	V_{pore} ($cm^3\ g^{-1}$)	Absorption edge (nm)	E_g (eV)	Emission peak (nm)	C : N ratio
bulk-U	23	0.027	419	2.856	438	3 : 4.7
U400-2	49	0.081	413	2.900	438	3 : 4.7
U425-2	67	0.123	415	2.881	438	3 : 4.6
U450-2	124	0.271	414	2.895	440	3 : 4.6
U450-4	209	0.400	414	2.891	440	3 : 4.6
U450-6	279	0.679	416	2.869	444	3 : 4.6

this region, in the 3100–3600 cm^{-1} range, the stretching vibration modes of N–H and N–H_2 bonds are distinguishable, indicating the presence of primary and/or secondary amino functional groups. The band displayed at 1623 cm^{-1} corresponds to the NH_2 bending vibration, and the band at 1540 cm^{-1} is assigned to the C=N stretching vibrations of the aromatic ring. Besides, the bands centred at 1397, 1314 and 1227 cm^{-1} are related to the stretching and rotation vibrations of the C–N of the heptazine rings. Finally, at lower frequencies, the narrow band at around 810 cm^{-1} is associated with the out-of-plane vibration of the heptazine ring group.[19,20]

Table 3 shows the C : N molar ratio of the materials, obtained by elemental analysis. The complete polymerization of the urea precursor to g-C_3N_4, would lead to a C : N ratio of 3 : 4. However, all the materials show a lower ratio, which is related to incomplete polymerization and oxidation of the carbon nitride structure. In addition, no significant differences in the C : N ratio could be observed despite the variation in the exfoliation conditions. This result indicates that the thermal treatment does not substantially affect the ratio between carbon and nitrogen content of the urea-derived materials, in agreement with previous reports.[21]

The morphology and structure of C_3N_4 materials were investigated by scanning electron microscopy (SEM) and transmission electron microscopy (TEM). The SEM image of the bulk sample (Fig. 6a) displays disordered solid agglomerates, giving rise to a morphology formed by criss-cross smooth blocks. After the thermal treatment at 450 °C (U450-6) (Fig. 6b),

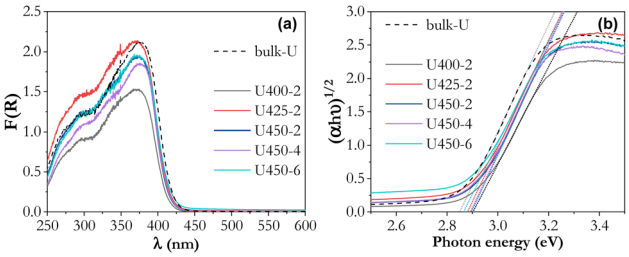

Fig. 8 (a) UV-Vis DR spectra and (b) Tauc plot to calculate the band gap energy of the synthesised materials.

the surface of the aggregates is less smooth evidencing an irregular delamination of the structure compared to the reference material. In addition, the high-magnification of this image (Fig. 6c) reveals that the 2D nanosheets tend to bend, making curled in-plane edges to minimize the surface free energy.[7,18]

In the TEM micrographs, the parent bulk-U (Fig. 7a) displays a marked agglomeration of disordered layers with numerous in-plane voids, which some authors have related to the release of ammonia gas during the synthesis process.[22] After thermal etching at 400 °C for 2 h (U400-2), the nanosheets appeared as large curved layers, as shown in Fig. 7b. In agreement with the SEM images and previous reports, the edges of the layers tend to bend to reduce surface energy.[19] The further increase in time and temperature (Fig. 7c) causes a much lower degree of agglomeration and a smaller thickness of the sets of stacked layers (~10 nm), which is indicative of a fewer number of piled-

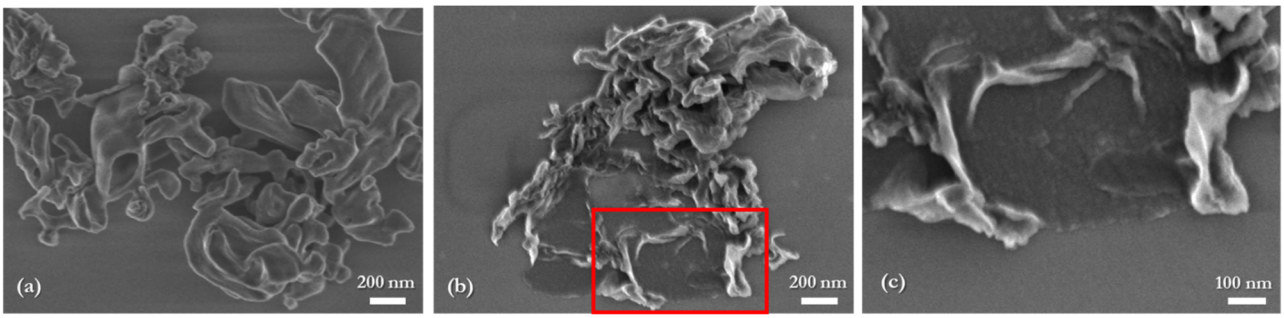

Fig. 6 SEM images of (a) bulk-U and (b) U450-6 and (c) high-magnification of the area included in the red box.

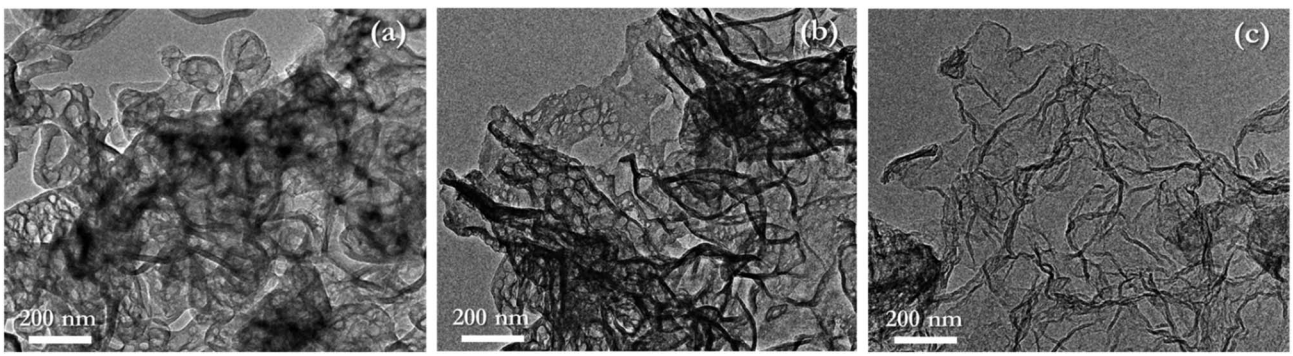

Fig. 7 TEM images of (a) bulk-U and the exfoliated materials (b) U400-2 and (c) U450-6.

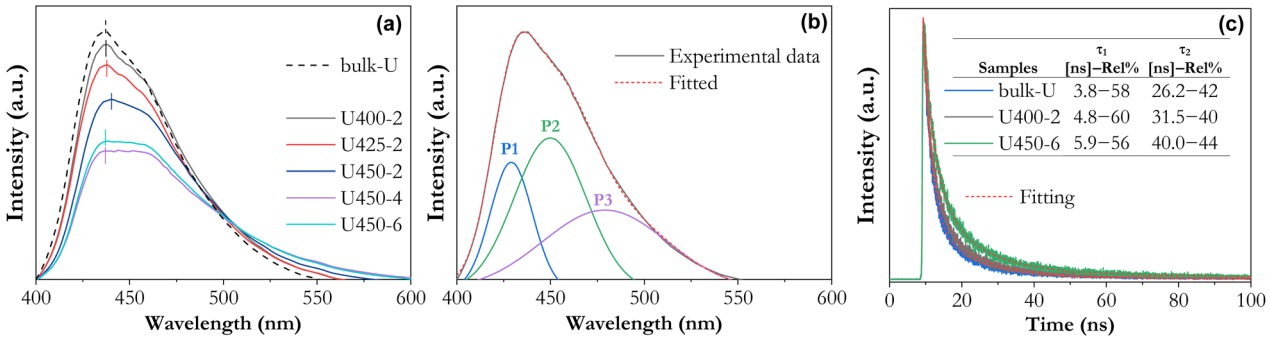

Fig. 9 (a) PL spectra of the bulk-U reference and exfoliated materials, (b) profile analysis by Gaussian fitting for bulk-U and (c) time-resolved fluorescence decay spectra monitored at 430 nm under 350 nm excitation for bulk-U, U400-2 and U450-6.

up layers. This is consistent with the increase in the surface area of the material (Table 3) and the decrease in the intensity of the X-ray diffraction signal at $2\theta = 27.4°$, compared to bulk-U (Fig. 5a and b).

The UV-Vis DR spectra of bulk-U and the exfoliated materials showed their absorption in the blue region of the visible spectra with a maximum in the UVA region at 378 nm (Fig. 8a). Table 3 lists the band gap values (E_g) calculated from the Tauc plot displayed in Fig. 8b. As can be observed, there is no significant change in the E_g values with varying the exfoliation conditions. This result is in agreement with those reported by other authors who also used urea as a g-C_3N_4 precursor and found that the band gap of the bulk material, *ca.* 2.80 eV, was just slightly increased to 2.88 eV by the exfoliation treatment.[22,23] In contrast, the band gap variations using other precursors (*e.g.*, melamine or thiourea) tend to be more pronounced when the material is exfoliated, increasing by more than 0.4 eV.[24,25]

PL spectra were used as an approach to qualitatively evaluate the extent of recombination of photogenerated electron–hole pairs. In general, a high PL emission denotes a significant recombination of the charge carriers. As shown in Fig. 9a, the PL spectra display a broad emission in the range of 400 to 600 nm.

Gaussian fitting to the photoluminescence profile was carried out to identify the constituents of this emission (Fig. 9b), obtaining three main bands centred at around 429, 450, and 480 nm, which is in accordance with previous studies that assigned them to transitions between the sp^3 C–N σ band, the sp^2 C–N π band, and the lone pair (LP) of the bridge nitride atom states, specifically, to σ* σ*–LP, π*–LP, and π*–π transitions, respectively.[26]

Fig. 9a also shows that the emission intensity gradually decreased from bulk-U to the materials exfoliated at increasing temperature and time. The decrease of the PL emission peak is indicative of a progressive suppression of the radiative electron–hole recombination in the exfoliated materials, hence favouring a higher lifetime of the charge carriers as the extent of the exfoliation increases (U450-4 and U450-6).[14] To further elucidate this, the time-resolved fluorescence decay profiles were measured and fitted to a bi-exponential decay function, and radiative lifetimes (τ_1 and τ_2) and the relative percentages of photoexcited charge carriers were determined (Fig. 9c). The shortest lifetime (τ_1) increased from 3.8 ns (bulk-U) to 4.8 ns and 5.9 ns when the material was exfoliated by thermal etching for 2 h at 400 °C (U400-2), and 6 h at 450 °C (U450-6), respectively. The same trend was observed for τ_2, which increased from 26.2 ns (bulk-U) to 31.5 ns (U400-2) and 40.0 ns (U450-6), respectively. The observed increase in the lifetime of the charge carriers as the degree of exfoliation increases, also reported in previous studies, can be related to the improved electron transport.[7,28] The development of intralayer mesoporosity and the decrease in the layer thickness promoted by the exfoliation (Fig. 5, 6 and 7) might facilitate the transport of charge carriers to the surface thus avoiding their recombination.[24,27] Therefore, the more successful the g-C_3N_4 exfoliation, the higher the expected photocatalytic activity, as the experimental results show (Table 1).

4. Conclusion

In the present work, a systematic approach using a 3^2 factorial experimental design was carried out to investigate the influence of the exfoliation temperature and time of bulk g-C_3N_4 obtained from urea (bulk-U) on the photocatalytic performance for methylparaben degradation. The results showed a significant influence of the exfoliation variables: the higher the temperature and time of the bulk thermal treatment, the better the resulting photocatalytic performance. The upper limit of both variables was, however, determined by the thermal stability of the bulk-U, and it was established at 450 °C and 6 h to avoid a low percent mass yield in the synthesis of the photocatalysts. The estimation of the costs related to the synthesis stage and the photocatalytic procedure at the laboratory scale pointed out the exfoliated material U450-2 as the one that minimises the energetic cost of the synthesis process, without compromising its photocatalytic activity, with a *ca.* 60% reduction in the cost of the whole process compared to the most active material (U450-6).

The physicochemical and optical characterization of the bulk and exfoliated materials demonstrated that the photocatalytic enhancement observed by increasing the exfoliation temperature and time can be mainly related to the significant

increase in the surface area, from 23 to 279 $m^2 g^{-1}$, caused by the breaking of the layer stacking in the carbon nitride structure whereas no significant modification of the band gap value or C to N ratio was induced by the thermal treatment. The sheet unpacking also led to an improvement in the separation of the photogenerated charge pairs, therefore contributing to the increase in the photocatalytic performance.

Author contributions

The three listed authors have substantially contributed to this work. Jorge Plaza: investigation; conceptualization; methodology; visualization; writing – original draft. Amaya Arencibia: investigation; conceptualization; supervision; validation; visualization; writing – review & editing. María-José López-Muñoz: investigation; conceptualization; supervision; validation; visualization; writing – review & editing; funding acquisition.

Conflicts of interest

There are no conflicts to declare.

Acknowledgements

The authors gratefully acknowledge the financial support of Agencia Estatal de Investigación (AEI) and Ministerio de Ciencia e Innovación through the project, AQUAENAGRI (PID2021-126400OB-C32) and the European Union's Horizon 2020 research and innovation program under the Marie Skłodowska-Curie grant agreement no. 101007578, SusWater project.

References

1 A. Sudhaik, P. Raizada, P. Shandilya, D. Y. Jeong, J. H. Lim and P. Singh, *J. Ind. Eng. Chem.*, 2018, **67**, 28–51.
2 N. F. F. Moreira, M. J. Sampaio, A. R. Ribeiro, C. G. Silva, J. L. Faria and A. M. T. Silva, *Appl. Catal., B*, 2019, **248**, 184–192.
3 J. Zhang, J. Sun, K. Maeda, K. Domen, P. Liu, M. Antonietti, X. Fu and X. Wang, *Energy Environ. Sci.*, 2011, **4**, 675–678.
4 J. Wen, J. Xie, X. Chen and X. Li, *Appl. Surf. Sci.*, 2017, **391**, 72–123.
5 G. Li, L. Li, H. Yuan, H. Wang, H. Zeng and J. Shi, *J. Colloid Interface Sci.*, 2017, **495**, 19–26.
6 M. J. Lima, A. M. T. Silva, C. G. Silva and J. L. Faria, *J. Catal.*, 2017, **353**, 44–53.
7 P. Niu, L. Zhang, G. Liu and H. M. Cheng, *Adv. Funct. Mater.*, 2012, **22**, 4763–4770.
8 C. Haman, X. Dauchy, C. Rosin and J.-F. Munoz, *Water Res.*, 2015, **68**, 1–11.
9 L. Sun, T. Yu, J. Guo, Z. Zhang, Y. Hu, X. Xiao, Y. Sun, H. Xiao, J. Li, D. Zhu, L. Sai and J. Li, *Sci. Rep.*, 2016, **6**, 1–9.
10 T. Li, L. Zhao, Y. He, J. Cai, M. Luo and J. Lin, *Appl. Catal., B*, 2013, **129**, 255–263.
11 A. Thomas, A. Fischer, F. Goettmann, M. Antonietti, J.-O. Müller, R. Schlögl and J. M. Carlsson, *J. Mater. Chem.*, 2008, **18**, 4893.
12 Y. Kang, Y. Yang, L. C. Yin, X. Kang, G. Liu and H. M. Cheng, *Adv. Mater.*, 2015, **27**, 4572–4577.
13 O. S. Arvaniti, A. Petala, A. A. Zalaora, D. Mantzavinos and Z. Frontistis, *J. Chem. Technol. Biotechnol.*, 2020, **95**, 2811–2821.
14 Y. Kang, Y. Yang, L. C. Yin, X. Kang, L. Wang, G. Liu and H. M. Cheng, *Adv. Mater.*, 2016, **28**, 6471–6477.
15 F. Fina, S. K. Callear, G. M. Carins and J. T. S. Irvine, *Chem. Mater.*, 2015, **27**, 2612–2618.
16 A. N. Oliveros, J. A. I. Pimentel, M. D. G. de Luna, S. Garcia-Segura, R. R. M. Abarca and R. A. Doong, *Chem. Eng. J.*, 2021, **403**, 126213.
17 I. Papailias, N. Todorova, T. Giannakopoulou, N. Ioannidis, N. Boukos, C. P. Athanasekou, D. Dimotikali and C. Trapalis, *Appl. Catal., B*, 2018, **239**, 16–26.
18 Q. Gu, Z. Gao, H. Zhao, Z. Lou, Y. Liao and C. Xue, *RSC Adv.*, 2015, **5**, 49317–49325.
19 F. Dong, Z. Wang, Y. Sun, W.-K. Ho and H. Zhang, *J. Colloid Interface Sci.*, 2013, **401**, 70–79.
20 C. Wu, S. Xue, Z. Qin, M. Nazari, G. Yang, S. Yue, T. Tong, H. Ghasemi, F. C. R. Hernandez, S. Xue, D. Zhang, H. Wang, Z. M. Wang, S. Pu and J. Bao, *Appl. Catal., B*, 2021, **282**, 119557.
21 T. V. de Medeiros, A. O. Porto, H. A. Bicalho, J. C. González, R. Naccache and A. P. C. Teixeira, *J. Mater. Chem. C*, 2021, **9**, 7622–7631.
22 X. Li, H. Zhang, J. Huang, J. Luo, Z. Feng and X. Wang, *Ceram. Int.*, 2017, **43**, 15785–15792.
23 Y. Yang, J. Chen, Z. Mao, N. An, D. Wang and B. D. Fahlman, *RSC Adv.*, 2017, **7**, 2333–2341.
24 Y. Li, M. Q. Wang, S. J. Bao, S. Lu, M. Xu, D. Long and S. Pu, *Ceram. Int.*, 2016, **42**, 18521–18528.
25 F. Dong, Y. Li, Z. Wang and W. K. Ho, *Appl. Surf. Sci.*, 2015, **358**, 393–403.
26 Y. Yuan, L. Zhang, J. Xing, M. I. B. Utama, X. Lu, K. Du, Y. Li, X. Hu, S. Wang, A. Genç, R. Dunin-Borkowski, J. Arbiol and Q. Xiong, *Nanoscale*, 2015, **7**, 12343–12350.
27 L. Shi, L. Liang, F. Wang, J. Ma and J. Sun, *Catal. Sci. Technol.*, 2014, **4**, 3235–3243.
28 Y. Li, R. Jin, Y. Xing, J. Li, S. Song, X. Liu, M. Li and R. Jin, *Adv. Energy Mater.*, 2016, 1601273.

